Extensive release of methane from Arctic seabed west of Svalbard during summer 2014 does not influence the atmosphere

C. Lund Myhre[1], B. Ferré[2], S. M.Platt[1], A. Silyakova[2], O. Hermansen[1], G. Allen[3], I. Pisso[1], N. Schmidbauer[1], A. Stohl[1], J. Pitt[3], P. Jansson[2], J. Greinert[8,2], C. Percival[3], A. M. Fjaeraa[1], S. O'Shea[3], M. Gallagher[3], M. Le Breton[3], K. Bower[3], S. Bauguitte[7], S. Dalsøren[4], S. Vadakkepuliyambatta[2], R. E. Fisher[6], E.G. Nisbet[6], D. Lowry[6], G.Myhre[4], J. Pyle[5], M. Cain[5], J. Mienert[2]

1 NILU - Norwegian Institute for Air Research, PO Box 100, 2027 Kjeller, Norway

2 CAGE-Centre for Arctic Gas Hydrate, Environment and Climate, Department of Geology, University of Tromsø, 9037 Tromsø, Norway

3 School of Earth, Atmospheric and Environmental Science, University of Manchester, Oxford Rd, Manchester, M13 9PL, UK.

4 Center for International Climate and Environmental Research – Oslo (CICERO), Pb. 1129 Blindern, 0318 Oslo, Norway

5 National Centre for Atmospheric Science, Department of Chemistry, University of Cambridge, Lensfield Road, Cambridge CB2 1EW, UK

6 Royal Holloway, University of London, Egham, Surrey, TW20 0EX, UK

7 Facility for Airborne Atmospheric Measurements (FAAM), Building 125, Cranfield University, Cranfield, Bedford, MK43 0AL, UK

8 GEOMAR, Helmholtz-Zentrum für Ozeanforschung, Wischhofstr. 1-3, 24148 Kiel, Germany

Corresponding author: Cathrine Lund Myhre (clm@nilu.no)

Key Points:

- Summer 2014 CH_4 release from seabed sediments west of Svalbard substantially increases CH_4 concentrations in the ocean, but not in the atmosphere
- The maximum flux to the atmosphere compatible with the observed atmospheric CH_4 mixing ratios is 2.4-3.8 nmol m^{-2} s^{-1} from 20 June – 1 August 2014
- Ay ocean-atmosphere flux of the CH_4 accumulated beneath the pycnocline may only occur if physical processes remove this dynamic barrier

Abstract

We find that summer methane (CH_4) release from seabed sediments west of Svalbard substantially increases CH_4 concentrations in the ocean, but has limited influence on the atmospheric CH_4 levels. Our conclusion stems from complementary measurements at the sea floor, in the ocean, in the atmosphere from land-based, ship and aircraft platforms during a summer campaign 2014. We detected high concentrations of dissolved CH_4 in the ocean above the seafloor with a sharp decrease above the pycnocline. Model approaches taking potential CH_4 emissions from both dissolved and bubble released CH_4 from a larger region into account, reveal a maximum flux compatible with the observed atmospheric CH_4 mixing ratios of 2.4-3.8 nmol m^{-2} s^{-1}. This is too low to have an impact on the atmospheric summer CH_4 budget in the year 2014. Long-term ocean observatories may shed light on the complex variations of Arctic CH_4 cycles throughout the year.

1 Introduction

The important greenhouse gas methane (CH_4) has large natural sources vulnerable to climate change [Ciais et al., 2013, Myhre et al., 2013, Portnov et al., 2016]. The causes of the recent global average growth of ~6 ppb year^{-1} since 2007 in atmospheric CH_4, including a marked Arctic growth event in 2007, remain unclear [Nisbet et al, 2014, Kirschke et al. 2013]. Decomposing methane hydrates (MHs) in marine sediments along continental margins are potentially a large natural source [Ruppel et al 2011]. How much of the CH_4 stored or formed by biogenic processesin the Arctic subsea that escapes to the atmosphere remains an open question. Large CH_4 gas escape from the shallow seabed into the ocean column has been reported from East Siberian shelves, particularly during storms [Shakhova et al., 2014], and from the Laptev and Kara Seas [Shakhova et al. 2010, Portnov et al., 2013]. Very high fluxes of CH_4 from sub-seabed sources to the atmosphere have been reported for the East Siberian Arctic Shelf (ESAS) [Shakhova et al. 2014, 2010], with flux values of ca. 70-450 nmol m^{-2} s^{-1} under windy conditions, with a postulated average total area (extrapolated) source magnitude of 17 Tg year^{-1} representing 3% of the global budget to the atmosphere. However, on the contrary it was recently found that ESAS region only emits from 0.5 to 4.5 Tg year^{-1} (Berchet et al. 2016). Based on continuous atmospheric observations.There are hundreds of gas plumes observed in the water, suggestive of gas release north-west off Svalbard. Along the West Svalbard continental margin, extensive gas bubbling from the sea floor has been observed in shallow water at 90-400 m depth [this work, Knies et al., 2004; Westbrook et al, 2009; Rajan et al., 2012, Sahling et al., 2014; Veloso et al., 2015; Graves et al., 2015; Steinle et al., 2015, Portnov et al., 2016] outside of today's gas hydrate stability zone [Panieri et al., 2016]. It is unknown how much of the CH_4 flux from the marine sediments in this region ultimately reaches the atmosphere [Fisher et al., 2011], either through bubbles or flux of dissolved CH_4.

The amount of CH_4 stored within gas hydrates, or as dissolved and free gas, north of 60^{o}N is uncertain. Estimates as high as 1200 Gt have been reported [Biastoch et al 2011]. Some hydrate deposits may be on the verge of instability due to ocean warming, leading to a debate whether CH_4 release could trigger positive feedback and accelerate climate warming [Archer, 2007, Isaksen et al, 2011; Ferré et al., 2012]. There have been very few studies aimed at detecting and quantifying the potential atmospheric enhancement of this oceanic source around Svalbard, and estimating their fluxes contributions. The West Svalbard continental margin is warmed by the northward flowing West Spitsbergen Current, the northernmost limb of the Gulf Stream. There has been an increase in the bottom water temperature in this area of 1.5 ºC [Ferré et al, 2012] over the last 30 years, while the atmosphere has warmed by as much as 4 ºC since the early 1970s [Nordli et al, 2014]. Continued warming in this region is expected [Collins et al, 2013]. Consequently, it is crucial to determine whether, and how, CH_4 from the shallow shelf located close to a stable gas hydrate zone on the upper continental margin reaches the atmosphere at present, and how this might change in the future. To investigate this we have conducted an intensive atmospheric and oceanographic survey (Figure 1) in an area with a known high density of hydroacostically detected gas flares (indications of bubbles in echograms) west of Prins Karls Forland, Svalbard, from 23 June to 2 July 2014, with atmospheric measurements continuing to 1 August. We investigated whether there was an atmospheric enhancement and impact during summer time. The measurements were used in combination with three different models to provide independent top down flux constraints, also taking into account potential emissions from larger areas outside the focused campaign region for the period.

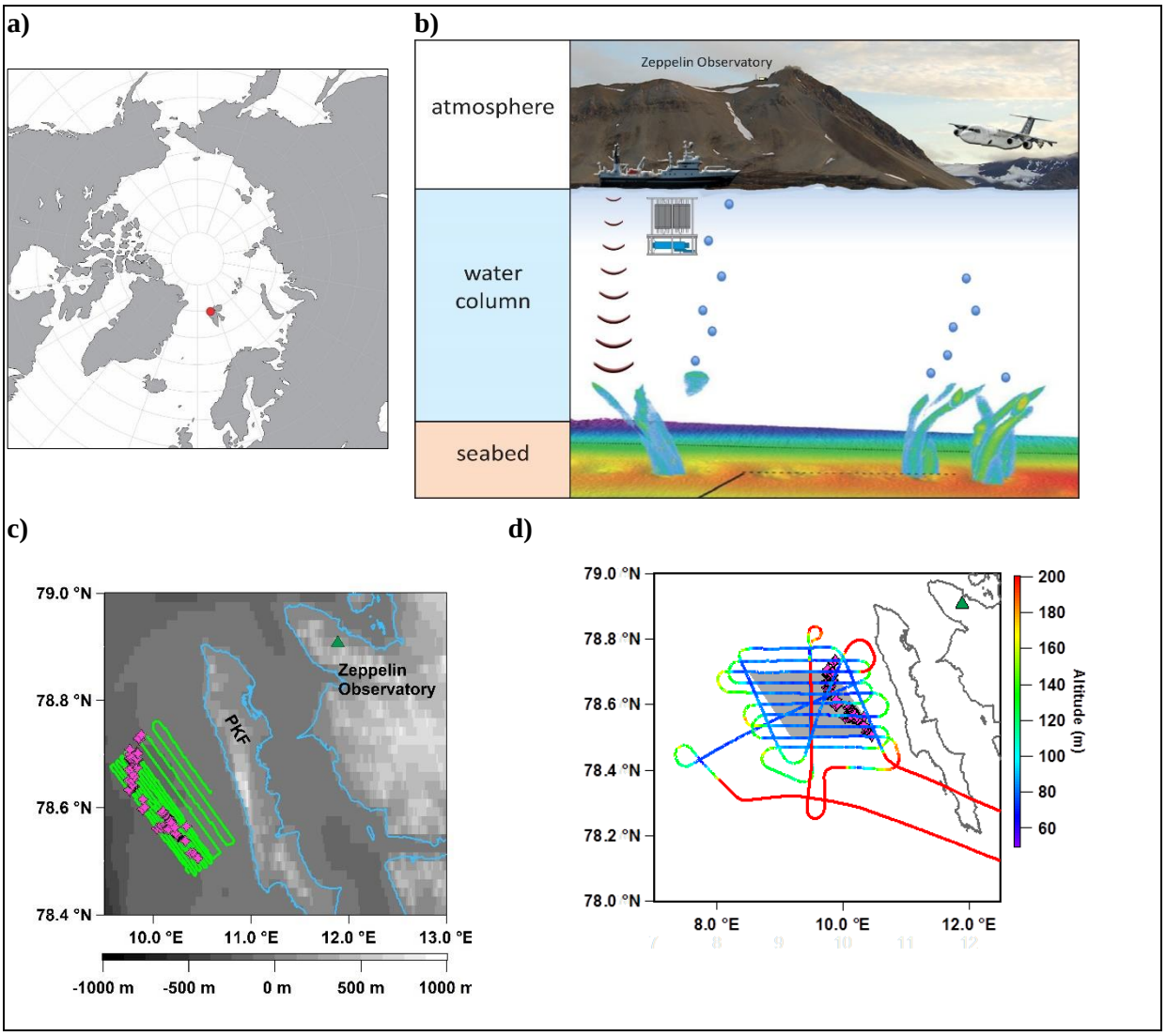

Figure 1: Field campaign and measurement platforms at the sea floor, in the water column, and in the atmosphere west of Svalbard in June-July 2014. a) The location of the measurement area marked in red west of Svalbard. b) Illustration of the field activity from 23 June to 2 July (not to scale) 2014. Seeps on the seafloor, represented here by swath bathymetry, release gas bubbles that rise through the water column. The Research Vessel Helmer Hanssen detected gas bubbles and collected water samples at various depths, and provided online atmospheric CH_4, CO and CO_2 mixing ratios and discrete sampling of complementary trace gases and isotopic ratios. The Facility of Airborne Atmospheric Measurements (FAAM) aircraft measured numerous gases in the atmosphere, and an extended measurement program was performed at the Zeppelin Observatory close to Ny-Ålesund. c) Detailed map of the area of intense ship-borne measurements. The ship track (green line) covers an Arctic shelf region, ~80-200 m depth, as indicated by bathymetric data west of Prins Karls Forland (PKF), an area with numerous observed flares [Westbrook et al, 2009; Sahling et al., 2014; and this work, shown as pink symbols]. The location of the Zeppelin observatory is shown (green triangle), ~50 km from PKF. d) Flight track over the same region on 2nd July; altitude is given by the colour scale, and the area used for the flux calculation based on flight data is shown in grey.

2 Data and Methodology

2.1 Field platforms, measurements and data

An overview of the area together with the complementary measurement platforms is presented in Figure 1. The Research Vessel (RV) Helmer Hanssen was equipped with instruments to analyse water samples from the sea surface down to the seabed and to monitor CH_4 atmospheric mixing ratios from 20 June an onwards. A single-beam echosounder constantly recorded flares in echograms; flares represent locations where bubbles are released from the seafloor which rise through the water column [Veloso et al., 2015], and where we expect high dissolved CH_4 concentrations. Figure 1c shows the ship's route during 24 -27 June 2014, together with identified gas flares. Aircraft measurements during the campaign were performed as low as ~15 m above the ocean, covering a larger area than the ship, for a short time (flights were around 4 h in duration). Figure 1d shows the 'Facility of Airborne Atmospheric Measurements' (FAAM) aircraft path and height on 2 July 2014 in the area, and the location of the flares identified [see Pitt et al., 2016; O'Shea et al, 2013; Allen et al., 2011 for details of the aircraft and instrumentation]. Finally, measurements of the atmospheric composition at the nearby Zeppelin Observatory include continuous CH_4 measurement and daily sampling of CH_4 isotopic ratios, amongst others (see Table S1); Figure S1 shows the locations. A description of all instruments and methods employed is included in the supplementary information. Table S1 gives an overview of the instruments from all platforms involved.

2.2 Model tools for data analysis and top-down flux estimations

Potential CH_4 seep locations around Svalbard were determined by MH stability modelling. The MH stability model (CSMHYD program, Sloan and Koh, 2008) was used taking bottom water temperatures (World Ocean Database, 2013) and sediment thermal gradients (Global Heatflow Database) from around Svalbard as input parameters. Locations where the hydrate stability zone outcrops at the seabed, are considered to be potential CH_4 seep locations. These locations were supplemented with all known CH_4 seeps [this work, Sahling et al., 2014, Panieri et al, 2015]. The modelled potential methane seep locations and known methane seeps are illustrated in Figure 2 as light blue and red dots, respectively.

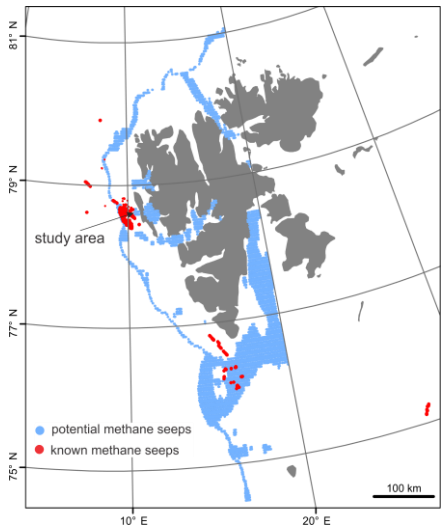

Figure 2: The identified (red) and potential (blue) seep locations around Svalbard as calculated by methane hydrate stability modelling.

In order to estimate CH_4 fluxes from the modelled seep area (blue in Figure 2) and identified CH_4 seep areas (red in Figure 2), we used three different independent atmospheric models; [1)] the Lagrangian particle dispersion model FLEXPART [Stohl et al., 2005], [2)] the global chemical transport model Oslo CTM3 [Søvde et al., 2012, Dalsøren et al., 2016], and [3)] a Lagrangian mass balance box model [Karion et al., 2013; O'Shea et al. 2014]. See section S3 for details about models and simulations.

3 Results and Discussion

3.1 Observations in the ocean and atmosphere

We present the results following the methane migration path from the sea floor through the water column into the lowermost atmosphere close to the sea surface (ship) and higher up using flight data covering a larger area. Figure 3 illustrates the dissolved CH_4 concentrations sampled over the investigated area. Elevated concentrations were found around the most extended cluster of flares and the CH_4 distribution shows a rapid change at about ~50 m water depth, with the highest dissolved CH_4 concentrations near the seafloor ~150 m depth. Little CH_4 is found above the pycnocline (boundary where the density gradient is greatest, affected by temperature and salinity), but sea surface CH_4 concentrations are still oversaturated with respect to atmospheric concentrations in a few places eastward, close to the shore

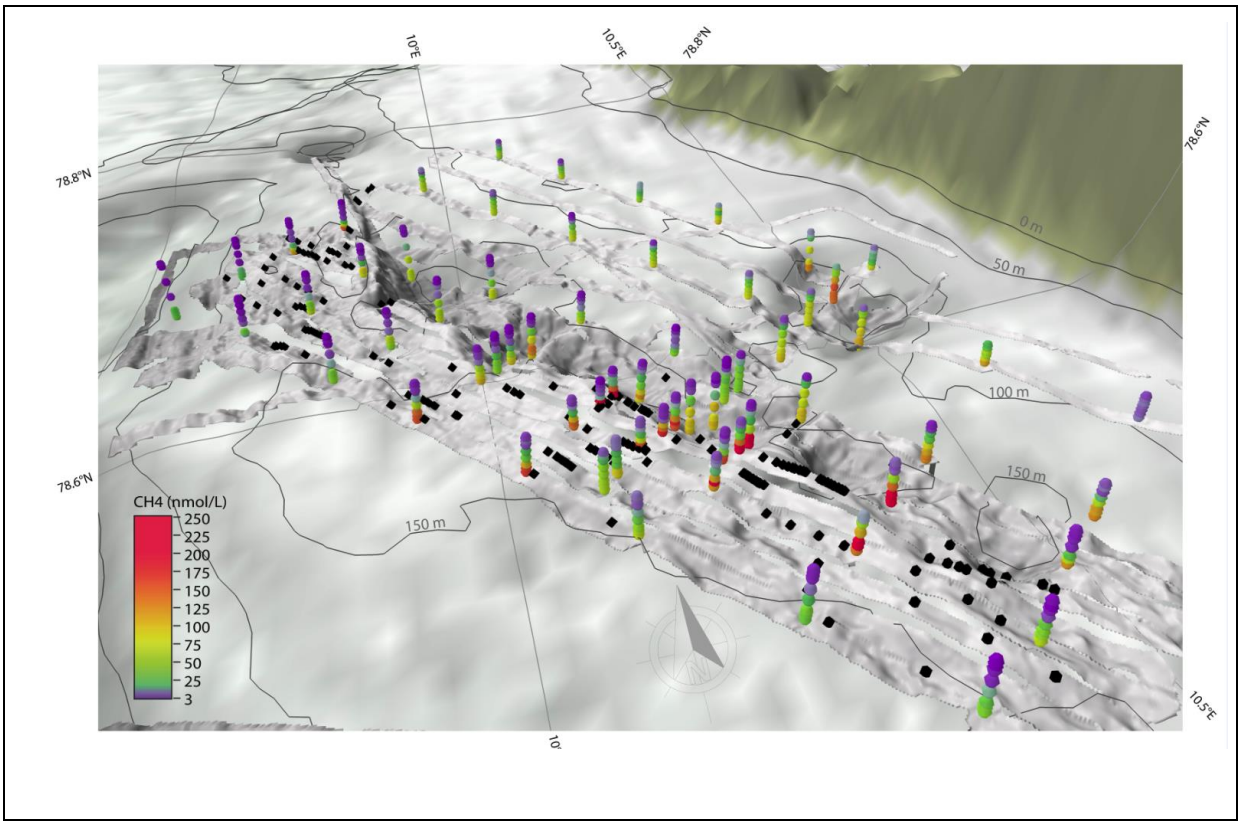

Figure 3: CH_4 concentrations from a hydrocast survey offshore of Prins Karls Forland. The first three bottles were taken 5, 15 and 30 meters above the seafloor and the last three bottles were taken 10, 20 and 30 meters below the sea surface. The rest of the samples were spread equally in the water column depending on the bottom depth. CH_4 concentrations in the ocean are illustrated by coloured dots (scale on the bottom left in nmol L^{-1}). Black dots indicate the location of the gas flares. Isobaths are from IBCAO v.3 grid and the superimposed higher resolution bathymetry is from the multi-beam survey performed during the RV Helmer Hanssen cruise, data were recorded over the period 25 June – 1 July 2014.

The sea-surface CH_4 ocean concentrations (Figure 4a) and the atmospheric mixing ratio measured by both the ship (Figure 4b) and the aircraft (Figure 4c) show very similar patterns. In the surface water CH_4 was generally <8 nmol L^{-1} (Figure 4a) with a median of 4.8 nmol L^{-1}. A maximum of 26 nmol L^{-1} was found near the shore, where no gas flares are found in the vicinity (Figure 4 a/b). The elevated surface water CH_4 concentrations coincide with a small increase (<2 ppb) of atmospheric CH_4 mixing ratio detected by the ship. This slightly elevated CH_4 close to the shore is probably not due to CH_4 released from the seafloor/seeps. Figure 3 and Figure 4 show that the bottom CH_4 concentrations are low in this coastal area. A simultaneous decrease in salinity suggests the intrusion of methane-enriched fresher water [Damm et al., 2005] increasing the dissolved sea surface-near CH_4 concentrations in this particular area.

A 6 km transect was sampled twice in one week by the *Helmer Hanssen* to monitor rapid variations of oceanographic conditions and their effects on the dissolved CH_4 distribution. The maximum bottom water CH_4 concentration doubled in one week from 200 to 400 nmol L^{-1} (see

Figure 4d and S2) while bottom water temperatures remained relatively stable. At the same time, the concentrations above the pycnocline and at sea surface remained relatively stable and low (4-11 nmol L^{-1} and ~10 nmol L^{-1} in the surface water on 24th June and 1st July, respectively).

This is in agreement with changes reported by Steinle et al, [2015] for bottom and sea surface water. This change in concentration can be explained either by slower advection during the later observations, or that the water was previously CH_4 enriched by an emission burst from one or several nearby seep sites. Gas bubble dissolution modelling from a previous study in the deeper area to the west of our study area, estimated that 80% of the bubble released CH_4 is dissolved below the summer pycnocline, and the remaining CH_4 is transported northwards where it is most likely oxidised by methanotrophic bacteria [Gentz et al, 2014, Steinle et al. 2015]. A similar conclusion came from a box modelling result of dissolved CH_4 indicating that ~60% of CH_4released at the seafloor becomes already oxidized before it reaches the overlying surface waters [Graves et al., 2015]. Although our single beam echosounder studies show bubbles reaching the sea surface, very little CH_4 remains in such bubbles by the time they reach the surface [Greinert and McGinnies, 2009].

We compared data from the RV Helmer Hansen to those from the Zeppelin observatory for the period from 20 June – 1 August. The CH_4 mixing ratio measured aboard the ship during the measurements off PKF agrees well with those recorded by the Zeppelin Observatory, as does the isotopic ratio (see Supplementary Figure S3). Our measurements above the flares were not influenced by long range transport of methane-enhanced-air masses from lower latitudes, as this would have produced noticeable transient enhancements in CH_4, as exemplified in Figure S3.

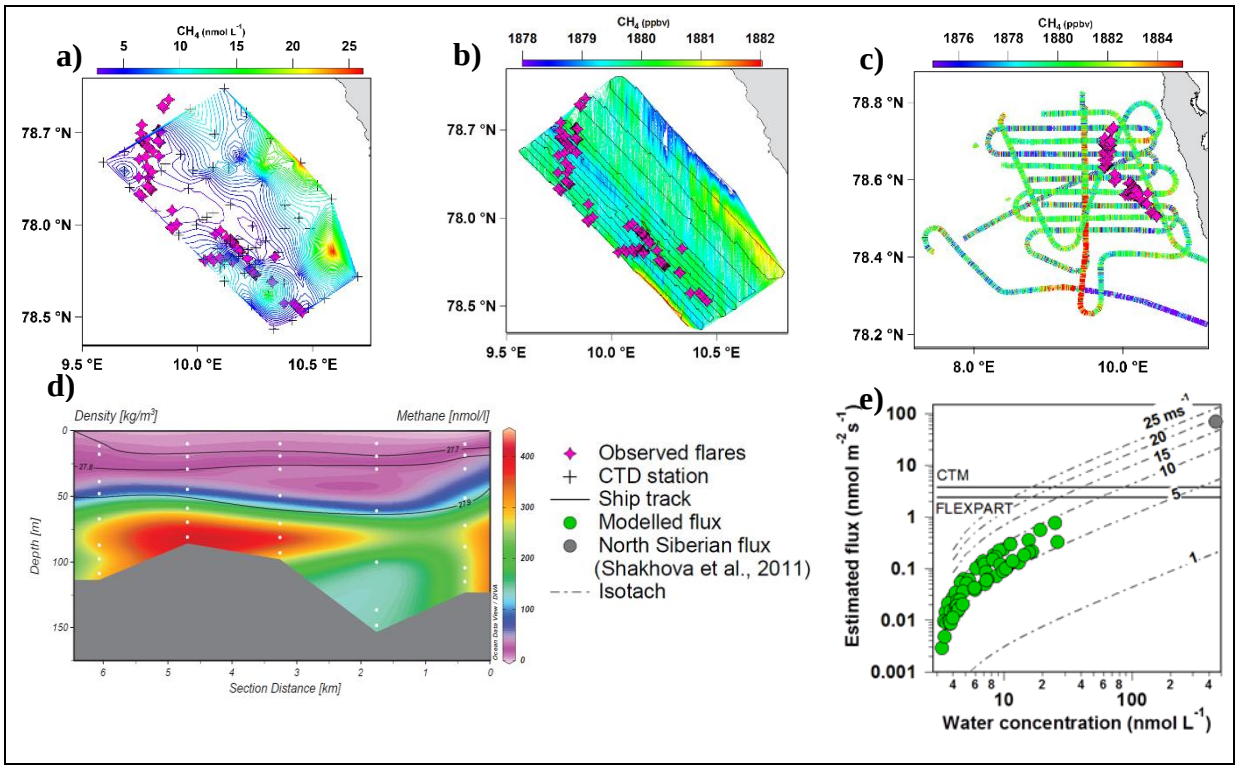

Figure 4: Comparison of CH_4 variations in the ocean and atmosphere west of Svalbard, and corresponding CH_4 flux to the atmosphere. a) Contour plot of near-surface CH_4 concentration (colour scale) at ~10 m depth in the water column. *CH_4* was measured by oceanographic conductivity/temperature/depth (CTD) stations (crosses) west of Prins Karls Forland (PKF). Observed flares are shown by pink markers. b) Contour plot of atmospheric CH_4 mixing ratio in ppb measured aboard RV Helmer Hanssen (colour scale). Ship track shown by black line, flares are shown by pink markers. c) CH_4 measured by the FAAM aircraft, flares are shown by pink markers. d) CH_4 concentration in the water column along a transect of CTD stations taken on 1st July 2014 showing a clear stratification of water masses with the pycnocline near 50 m water depth. Density is own as black contours. (The transect location offshore of Prins Karls Forland is shown in Figure S2, b). Panel e) CH_4 flux to the atmosphere at each CTD location as a function of ocean CH_4 concentration according to a diffusive model (green points). Flux previously modelled off Northern Siberia during stormy weather [Shakhova et al., 2011] is given by the grey point. Dashed lines show the model flux at different isotachs (lines of constant wind speed), assuming constant salinity and temperature (averaged over the sampling period used). Horizontal lines show the maximum possible flux constrained by the atmospheric measurements from the ship, according to FLEXPART and OsloCTM3 models. FLEXPART and CTM constraints are for the atmospheric sampling period 20 June – 1 Aug and will vary with weather patterns.

194

195 **3.2 Flux estimates from ocean to atmosphere in the Svalbard region during summer**

196 We estimate the median ocean-atmosphere CH_4 flux based on observations in the ocean, in
197 addition to 3 top-down constrain of the flux employing 3 independent models and the
198 atmospheric measurements.

199

We estimate a median ocean-atmosphere CH_4 flux of 0.04 nmol m^{-2} s^{-1} (σ = 0.13) from data at each *CTD* station using an ocean-atmosphere gas exchange function [Wanninkhof et al, 2009, Figure 4e]. The maximum flux at the CTD stations is 0.8 nmol m^{-2} s^{-1} which occurred when both dissolved CH_4 concentrations and wind speeds were high, 25 nmol L^{-1} and 9 m s^{-1} respectively. This model only considers air-sea exchange via diffusion of dissolved CH_4 and not the contribution of bubbles of gas reaching the surface. Figure 4e) shows the estimated flux at different wind speeds, assuming constant salinity and temperature (average from the campaign). Wind speed has a large effect: an increase from 5 to 10 ms^{-1} increases the modelled flux by almost an order of magnitude. The atmospheric CH_4 air mixing ratios aboard the RV Helmer Hanssen and at Zeppelin before, during, and after the ship-based measurements off Prins Karls Forland were very similar, with small variations (Figure 4e/b). Hence, the CH_4 air mixing ratios above active seep areas were representative of wider regional atmospheric concentrations, with no elevated levels or transient large increases.

To complement our observational based flux estimates of dissolved CH_4 we employed three independent atmospheric models to provide top-down constraints of the ocean-atmosphere flux, given the atmospheric concentrations sampled by the aircraft and the ship. This approach also take potential CH_4 from bubbles into account. We only detected a weak increase of 2 ppb in the atmospheric mixing ratio at the ship location close to bubbles, reflecting the potential enhancement from both dissolved CH_4 and CH_4 from bubbles. We calculated, using a Lagrangian transport model (FLEXPART), the CH_4 enhancements at the ship for all locations that would result from a 1 nmol $m^{-2}s^{-1}$ flux from the area, encompassing the identified and the potential CH_4 seep sites around Svalbard [Sahling et al., 2014, shown in Figure 2]. Running FLEXPART backwards in time for all ship positions over the period 20 June to 1 August, the modelled CH_4 enhancement is shown as the yellow line in the supplementary section, Figure S4; compared to the observations, no correlation (r^2=0.003) is evident. The most sensitive days are the highest 20% modelled peaks, (bold yellow line). Using the most sensitive days from this period we estimate a top down constraint on the flux from the seep areas of <2.4±1.3 nmol m^{-2} s^{-1}. This estimation assumes that all of the measured 2 ppb variation in the atmosphere is solely due to a flux from the modelled seep areas around Svalbard (Figure 2). Similarly, using a forward chemistry transport model (OsloCTM3, Søvde et al., 2012) a flux of 3.8 ±0.7 nmol m^{-2} s^{-1} was necessary to reproduce the 2 ppb increase in CH_4 at the ship, assuming the same emission region shown in Figure 2. This is equivalent to an annual emission of only 0.06 Tg for a constant flux throughout the year, very small compared to the total global annual emission of ca 600 Tg of CH_4, [Kirschke et al. 2013]. In addition, we used the aircraft measurements to provide another independent constrain on the maximum possible CH_4 flux in the region. The aircraft flew transects below 100 m altitude upwind and downwind of the potential seep sites, but observed no statistically significant change in CH_4 during these low level flights, see Figure 1d for altitudes. A Lagrangian mass balance calculation (similar to that employed by O'Shea et al., 2014) leads to an estimated flux of 3.0 ± 17.1 nmol m^{-2} s^{-1}. An estimated upper limit on the ocean-to-atmosphere CH_4 flux averaged over the grey shaded area shown in Figure 1d can then be quantified by the mean + 1σ value of 14.1 nmol m^{-2} s^{-1}. This represents the maximum possible flux for this area consistent with the aircraft CH_4 measurements and associated uncertainties.

FAAM aircraft measurements were also made in the same location off PKF in a previous MAMM campaign in summer 2012 as part of the UK Methane in the Arctic Measurement and Modelling project (MAMM – see Allen et al., 2014 for details). Similarly, any emission from the

seep areas was not detectable among the other signals in the aircraft data. Forward calculations, with a different dispersion model, led to very similar conclusions to those of 2014: that an emission flux of a few tens of nmol m^{-2} s^{-1} would have been required to detect the emission in the aircraft data [M. Cain, personal communication, 2016].

In sharp contrast to the flux calculations from the measurement-led approaches discussed here (Table 1), the flux reported by Shakhova et al. [2014] from the East Siberian Arctic Shelf is more than two orders of magnitude larger, 70-450 nmol m^{-2} s^{-1} under windy conditions, than our measurement-derived maximum for the period. Figure 4, panel e includes a comparison. Part of this large difference can be explained by both higher dissolved CH_4 concentrations in surface waters reported in the Siberian area (up to ~400 nmol L^{-1}) and the higher wind speeds reported by Shakhova et al. [2014]. Table 1 compiles our estimates of the spatially-averaged maximal flux in the region, as constrained by the atmospheric observations.

Table 1: Ocean to atmosphere CH_4 flux constraints offshore Prins Karls Forland from different independent methodologies. The potential flux region is shown in Figure 2, and employing atmospheric observation from Zeppelin and Helmer Hanssen over the period 20 June – 1 August 2014

Methodology	***Maximum flux possible constrained by the atmospheric observations*** **(nmol m^{-2} s^{-1})**
FLEXPART[a] top-down, backward modelling	*2.4 ± 1.4*
OsloCTM3[b] top-down forward modelling	*3.8 ± 1.4*
Lagrangian mass balancing - FAAM)[c], top-down, exploring up-wind/down-wind variations	*14.1*

[a] Lagrangian Particle Dispersion model [Stohl et al., 2005] [b] Chemical transport model [Søvde et al. 2012, Dalsøren et al 2016] [c] Lagrangian mass balance approach [Karion et al., 2013; O'Shea et al. 2014]. Note that the flux constrain based on the flight data is weaker; there was no statistically significant change in downwind CH_4 mixing ratio relative to the measured upwind background, and this is the maximum possible flux that is consistent with the atmospheric flight measurements and associated uncertainties.

4 Conclusion

Despite the obvious influence of seeps on dissolved CH_4 concentrations in the ocean west of Svalbard in June - July summer 2014, very little CH_4 reaches the atmosphere, neither as bubbles transported nor dissolved gas. The median wind speed was 6.6 m s^{-1} during our campaign, and the pycnocline remained stable. We suggest that dissolved methane captured below the pycnocline may only be released to the atmosphere when physical processes remove this dynamic barrier. In such a situation, dissolved CH_4 concentrations would rapidly decrease and any large flux would most likely be transient. Consequently, we conclude that large CH_4 releases to the atmosphere with strong impact on the atmospheric levels from sub-sea sources, including hydrates, do not occur to the west of Svalbard, presently. Shorter periods with large fluxes, particular during other times of the year such as during ice break-up or storm events, might

occur. The role of the pycnocline in this context will be investigated in more detail during long-term ocean observatory recordings in the future.

ACKNOWLEDGMENTS

The project **MOCA**- ***M****ethane Emissions from the Arctic* ***OC****ean to the* ***A****tmosphere: Present and Future Climate Effects* is funded by the Research Council of Norway, grant no.225814

CAGE – Centre for **A**rctic **G**as Hydrate**, E**nvironment and Climate research work was supported by the Research Council of Norway through its Centres of Excellence funding scheme grant no. 223259.

Nordic Center of Excellence **eSTICC** (**eS**cience **T**ool for **I**nvestigating **C**limate **C**hange in northern high latitudes) funded by Nordforsk, grant no. 57001.

Supporting Information

References

Allen, G., Coe, H., Clarke, A., Bretherton, C., Wood, R., Abel, S. J., Barrett, P., Brown, P., George, R., Freitag, S., McNaughton, C., Howell, S., Shank, L., Kapustin, V., Brekhovskikh, V., Kleinman, L., Lee, Y.-N., Springston, S., Toniazzo, T., Krejci, R., Fochesatto,J., Shaw, G., Krecl,P., Brooks, B., McMeeking, G., Bower, K. N., Williams, P. I., Crosier, J., Crawford I., Connolly, P., Allan, J. D., Covert, D., Bandy, A. R., Russell, L. M., Trembath, J., Bart, M., McQuaid, J. B., Wang, J., and Chand, D.: South East Pacific atmospheric composition and variability sampled along 20° S during VOCALS-REx, *Atmos. Chem. Phys*., 11, 5237-5262, doi:10.5194/acp-11-5237-2011, 2011.

Allen, G., Illingworth, S. M., O'Shea, S. J., Newman, S., Vance, A., Bauguitte, S. J.-B., Marenco, F., Kent, J., Bower, K., Gallagher, M. W., Muller, J., Percival, C. J., Harlow, C., Lee, J., and Taylor, J. P.: Atmospheric composition and thermodynamic retrievals from the ARIES airborne TIR-FTS system – Part 2: Validation and results from aircraft campaigns, Atmos. Meas. Tech., 7, 4401-4416, doi:10.5194/amt-7-4401-2014, 2014.

Archer, D. Methane hydrate stability and anthropogenic climate change. *Biogeosciences* **4,** 521–544 (2007).

Berchet, A., Bousquet, P., Pison, I., Locatelli, R., Chevallier, F., Paris, J.-D., Dlugokencky, E. J., Laurila, T., Hatakka, J., Viisanen, Y., Worthy, D. E. J., Nisbet, E., Fisher, R., France, J., Lowry, D., Ivakhov, V., and Hermansen, O.: Atmospheric constraints on the methane emissions from the East Siberian Shelf, Atmos. Chem. Phys., 16, 4147-4157, doi:10.5194/acp-16-4147-2016, (2016) 2016.

Biastoch, A. *et al.* Rising Arctic Ocean temperatures cause gas hydrate destabilization and ocean acidification. *Geophys. Res. Lett.* **38**, L08602, doi:10.1029/2011gl047222 (2011).

Bugna, G.C., J.P. Chanton, J.E. Young, W.C. Burnett and P.H. Cable. The importance of groundwater discharge to the methane budget of nearshore and continental shelf waters of the NE Gulf of Mexico Geochimica et Cosmochimica Acta, 60, 4735-4746 (1996).

Ciais, P. *et al.* Carbon and other biogeochemical cycles. In: *Climate Change 2013 – The Physical Science Basis*. pp. 465-570. Cambridge: Cambridge University Press (2014).

Collins, M. *et al.* Long-term climate change: projections, commitments and irreversibility. In: *Climate Change 2013 – The Physical Science Basis*. pp. 1029-1136. Cambridge: Cambridge University Press (2014).

Dalsøren, S. B., Myhre, C. L., Myhre, G., Gomez-Pelaez, A. J., Søvde, O. A., Isaksen, I. S. A., Weiss, R. F., and Harth, C. M.: Atmospheric methane evolution the last 40 years, *Atmos. Chem. Phys*., 16, 3099-3126, doi:10.5194/acp-16-3099-2016 (2016)

Damm, E., Mackensen, A., Budeus, G., Faber, E. & Hanfland, C. Pathways of methane in seawater: Plume spreading in an Arctic shelf environment (SW-Spitsbergen). *Continent. Shelf Res*. **25**, 1433–1452 (2005).

Ferré, B., Mienert, J. & Feseker, T. Ocean temperature variability for the past 60 years on the Norwegian-Svalbard margin influences gas hydrate stability on human time scales. *J. Geophys. Res.: Oceans* **117**, C10017, doi:10.1029/2012jc008300 (2012).

Fisher, R. E. *et al.* Arctic methane sources: Isotopic evidence for atmospheric inputs. *Geophys. Res. Lett.* 38**,** L21803, doi:10.1029/2011GL049319 (2011).

Gentz, T. *et al.* A water column study of methane around gas flares located at the West Spitsbergen continental margin, *Continent. Shelf Res.* **72,** 107–118 (2014).

Graves, C. A. et al. Fluxes and fate of dissolved methane released at the seafloor at the landward limit of the gas hydrate stability zone offshore western Svalbard. . *J. Geophys. Res.* Oceans **120,** doi:10.1002/2015JC011084 (2015).

Greinert, J. & McGinnis, D.F. Single bubble dissolution model - the graphical user interface SiBu-GUI. *Environ. Model. Software* **24**, 1012-1013 (2009).

Isaksen, I.S.A, Gauss, M., Myhre, G., Walter Anthony, K. M. & Ruppel, C. Strong atmospheric chemistry feedback to climate warming from Arctic methane emission. *Global Biogeochem. Cy.*, **25**, GB2002, doi:10.1029/2010GB003845 (2011).

Karion, A., *et al.* Methane emissions estimate from airborne measurements over a western United States natural gas field. *Geophys. Res. Lett.* **40**, 4393-4397 (2013).

Kirschke, S. *et al.* Three decades of global methane sources and sinks. *Nature Geosci.* **6**, 813-823 (2013).

Knies, J., Damm, E., Gutt, J., Mann, U. & Pinturier, L. Near-surface hydrocarbon anomalies in shelf sediments off Spitsbergen: Evidences for past seepages. *Geochem. Geophys. Geosyst.* **5,** Q06003, doi:10.1029/2003GC000687 (2004).

McGinnis, D. F., J. Greinert, Y. Artemov, S. E. Beaubien, and A. Wüest, Fate of rising methane bubbles in stratifiedwaters: How much methane reaches the atmosphere?, *J. Geophys. Res.,* **111**, C09007, doi:10.1029/2005JC003183 (2006).

Myhre, G. *et al.* Anthropogenic and natural radiative forcing. In: *Climate Change 2013 – The Physical Science Basis*. pp. 659-740. Cambridge: Cambridge University Press (2013).

Nisbet, E. G., Dlugokencky, E. J. & Bousquet, P. Methane on the rise — again. *Science* **343**, 493-495 (2014).

Nordlie, Ø, Przybylak, R., Ogilvie, A. E. J. & Isaksen, K. Long-term temperature trends and variability on Svalbard: the extended Svalbard Airport temperature series, 1898-2012. *Polar Res.* **33**, 21349, doi:10.3402/polar.v33.21349, 2014.

O'Shea, S. J., Bauguitte, S. J.-B., Gallagher, M. W., Lowry, D. & Percival, C. J. Development of a cavity-enhanced absorption spectrometer for airborne measurements of CH_4 and CO_2. *Atmos. Meas. Tech.* **6**, 1095-1109 (2013).

O'Shea, S. J. *et al.* Area fluxes of carbon dioxide, methane, and carbon monoxide derived from airborne measurements around Greater London: A case study during summer 2012. *J. Geophys. Res.: Atmos.* **119**, 4940-4952 (2014).

Panieri et al., Gas hydrate deposits and methane seepages offshore western Svalbard and Storfjordrenna: Biogeochemical and biological investigations, CAGE15-2 cruise report (2015).

Panieri, G., Graves, C.A., James, R.H., Paleo-methane emissions recorded in foraminifera near the landward limit of the gas hydrate stability zone offshore western Svalbard. G3, Geochemistry, Geophysics, Geosystems, DOI: 10.1002/2015GC006153 (2016).

Pitt, J. R. *et al*. The development and evaluation of airborne in situ N_2O and CH_4 sampling using a quantum cascade laser absorption spectrometer (QCLAS). *Atmos. Meas. Tech.* **9,** 63-77 (2016).

Portnov, A., Vadakkepuliyambatta, S., Mienert, J., Hubbard, A., Ice-sheet driven methane storage and release in the Arctic. Nature Communication; 7:10314, DOI: 10.1038/ncomms10314 (2016).

Portnov, A. *et al.* Offshore permafrost decay and massive seabed methane escape in water depths >20 m at the South Kara Sea shelf. *Geophys. Res. Lett.* **40,** 3962–3967 (2013).

Rajan, A., Mienert, J. & Bünz, S. Acoustic evidence for a gas migration and release system in Arctic glaciated continental margins offshore NW-Svalbard. *Mar. Petrol. Geol.* **32,** 36–49 (2012).

Ruppel, C. D. Methane hydrates and contemporary climate change. *Nature Education Knowledge* **3**,10, 29, http://www.nature.com/scitable/knowledge/library/methane-hydrates-and-contemporary-climate-change-24314790 (2011).

Sahling, H. *et al.* Gas emissions at the continental margin west of Svalbard: mapping, sampling, and quantification. *Biogeosciences* **11**, 6029-6046 (2014).

Shakhova, N. *et al.* Geochemical and geophysical evidence of methane release over the East Siberian Arctic Shelf. *J. Geophys. Res.* **115,** C08007, doi:10.1029/2009JC005602 (2010).

Shakhova, N. *et al.* Ebullition and storm-induced methane release from the East Siberian Arctic Shelf. *Nature Geosci.* **7,** 64–70 (2014).

Sloan, E. D. & Koh, C. A. Clathrate Hydrates of Natural Gases, Third Edition. Boca Raton, FL.: CRC Press (2008).

Smith, A.J., Mienert, J., Bünz, S. & Greinert, J. Thermogenic methane injection via bubble transport into the upper Arctic Ocean from the hydrate-charged Vestnesa Ridge, Svalbard. *Geochem. Geophys. Geosyst.* **15,** 1945-1959 (2014).

Steinle, L. *et al.* Water column methanotrophy controlled by a rapid oceanographic switch. *Nature Geosci.* **8**, 378-382 (2015).

Stohl, A., Forster, C., Frank, A., Seibert, P., & Wotawa, G. Technical note : The Lagrangian particle dispersion model FLEXPART version 6.2. *Atmos. Chem. Phys.* **5,** 2461-2474 (2005).

Søvde, O. A. *et al.* The chemical transport model Oslo CTM3. *Geosci. Model Dev.* **5,** 1441-1469 (2012).

Thompson, R. L., & Stohl, A. FLEXINVERT: an atmospheric Bayesian inversion framework for determining surface fluxes of trace species using an optimized grid. *Geophys. Mod. Dev.* **7,** 2223-2242 (2014).

Veloso, M., Greinert, J., Mienert, J. & De Batist, M. A new methodology for quantifying bubble flow rates in deep water using split beam echosounder: examples form the Arctic offshore NW Svalbard. *Limnol. Oceanogr. Meth.*, doi:10.1002/lom3.10024 (2015).

Westbrook, G. K. *et al.* Escape of methane gas from the seabed along the West Svalbard continental margin. *Geophys. Res. Lett.* **36**, L15608, doi:10.1029/2009gl039191 (2009).

Wanninkhof, R. *et al.* Advances in quantifying air-sea gas exchange and environmental forcing. *Annu. Rev. Marine. Sci.* **1,** 213-244 (2009).

441 Whitemann, G., Hope, C., & Wadhams, P. Climate science: Vast costs of Arctic change. *Nature*
442 **499**, 401–403 (2013).
443 Wiesenburg, D. A. & Guinasso, N. L. Jr. Equilibrium solubilities of methane, carbon monoxide,
444 and hydrogen in water and sea water. *J. Chem. Eng. Data* **24**, 356-360 (1979.)